ID-1384

THE BENDING AND TWISTING CONTROL OF SMA/GRAPHITE/EPOXY COMPOSITE BEAMS

Cheol Kim, Bum-Sik Park, and Nam-Seo Goo
Department of Mechanical Engineering, Kyungpook National University
Taegu, South Korea 702-701

ABSTRACT : Shape memory alloy (SMA) has demonstrated its potentials for various smart structure applications. SMA wires undergo a reversible phase transformation from martensite to austenite as temperature increases. This transformation leads to shape recovery and associated recovery strains. If SMA actuators are embedded off the neutral surface and are oriented in arbitrary angles with respect to a beam axis, then the beam bends and twists due to the coupling effects of recovery strains activated. In this study, the bending and twisting of a SMA/graphite/epoxy beam were controlled by both electric resistive heating and passive elastic tailoring. Three-dimensional finite element formulations were derived and validated to analyze the responses of the SMA/composite beam. Numerical results show that the shape of the SMA/graphite/epoxy composite beam can be controlled by judicious choices of control temperatures, SMA angles, and elastic tailoring.

KEYWORDS : Shape Memory Alloy, Shape Control, Composite Beam, Elastic Tailoring, Finite Element Method

INTRODUCTION

Over the years, smart materials and structures become very attractive in the development of innovative actuators, sensors, control systems, and adaptive structures. Their applications may dramatically improve the performances of various aerospace systems such as rotorcraft blades, aircraft wings, air inlets, engine nozzles, large deployable precision space systems, and robust micro-spacecraft [1]. Among several smart materials, the large strain recovery properties (up to 10%) of SMAs have let to many unique applications including uses as built-in-actuators for shape and vibration control of smart structures. Many constitutive equations have been proposed to represent the nonlinear SMA behaviors with hysteresis [2-4]. However, the efforts for the shape control of SMA-embedded composite structures are quite rare and, even if there exist some, the hosting materials were not structural [5-7]. Some works concerned with the dynamic responses of SMA structures [8,9].

When a composite beam is embedded with off-axis SMA wire actuators, the contraction of the wire activated by electric heating causes a distributed force to act upon the beam. Furthermore, if the actuator is not located on the neutral axis of the beam, the actuation force also results in a moment which causes the beam to bend and twist. Additionally, such deformations due to the recovery strain may be enhanced by using the concept of the elastic tailoring arising from the directional nature of hosting fibrous polymer composites [10]. The

proper elastic tailoring of composite lay-ups results in elastic coupling such as bending-twisting or extension-twisting couplings that strongly influence on the overall structural behavior.

In this paper, the behaviors of SMA and graphite/epoxy are formulated using the finite element method. It is then observed how the shape of elastically-tailored SMA/graphite/epoxy composite beams actively controlled by heating the SMA wires with appropriate electric currents. The influence of various lay-up angles of SMA wires and graphite fibers on the shape changes of the beam is also investigated by finite element analyses. The accuracy of the present formulation is compared with other analysis.

THEORETICAL FORMULATION

Behavior of Shape Memory Alloys

Shape memory materials undergo a transformation between an martensite and austenite phase. The factors that affect the phase transformation are known to be stress, strain, temperature, and history of transformation. The constitutive equation of a SMA wire can be developed based on these state variables. In this study, the following Brinson's one-dimensional model [4] is coupled into the composite beam as:

$$s - s_0 = D(x)e - D(x_0)e_0 + \Omega(x)x_0 - \Omega(x_0)x_{s_0} + \Theta(T - T_0) \tag{1}$$

$$D(x) = D_A + x(D_M - D_A) \tag{2}$$

$$\Omega(x) = -e_L D(x) \tag{3}$$

$$x = x_S + x_T \tag{4}$$

where s, e, D, Ω, Θ, x, and T are the stress, the strain, the modulus, the phase transformation coefficient, the thermal coefficient, the martensite fraction, and the temperature, respectively. The subscript "o" means the initial conditions, "s" means the stress induced variant, and "T" means the thermally induced variant.

As temperature increases, SMA wires show amazing abilities to recover large strain. If the recovery strain is constrained, the internal stress is induced. This internal stress generates actuating force. The recovery stresses in the SMA wires are assumed to consist of only an axial component.

Finite Element Formulation

The host materials of the beam consist of graphite/epoxy composites and are modeled with 8-noded three-dimensional elements. The governing equation for a SMA/graphite/epoxy composite body (Π) can be expressed as:

$$\int_{\Pi} s \cdot de d\Pi - \int_{\Pi} f \cdot du d\Pi - \int_{\Gamma} t \cdot du dS = 0 \tag{5}$$

where s, e, f, u, t, and Γ are the stress, the strain, the body force, the displacement, the surface traction, and the applied force boundary, respectively.
The coordinates, **x**, and displacements, **u**, can be expressed as follows, using interpolation functions,

$$\mathbf{x} = \begin{Bmatrix} X \\ Y \\ Z \end{Bmatrix} = \sum_{i=1}^{8} y_i \mathbf{x}_i, \qquad \mathbf{u} = \begin{Bmatrix} u_X \\ u_Y \\ u_Z \end{Bmatrix} = \sum_{i=1}^{8} y_i \mathbf{u}_i \tag{6}$$

and the shape functions are defined as follows,

$$y_i(x,h,z) = \frac{1}{8}(1+x_i x)(1+h_i h)(1+z_i z) \qquad i = 1,\cdots,8 \tag{7}$$

where the symbols x, h, and z are the natural coordinates, and the values x_i, h_i, and z_i are obtained at each node. Equation (5) is expressed as a following discrete function,

$$\left[K_{uu}^{e}\right]\left\{u^{e}\right\} = \left\{F^{e}\right\} \tag{8}$$

where

$$\mathbf{F}^{e} = \int_{\Gamma^{e}} \mathbf{H}^{T}\, \mathbf{t}\, dS, \qquad K_{uu}^{e} = \int_{V^{e}} B_i^{T} D B_j\, dV \tag{9}$$

SMA/Composite Model

The nonlinear finite element stiffness matrix of the SMA wire only is shown in [11] and represented as:

$$[K]^{e} = H\overline{D}A\int_{L}[B]^{T} F F^{T}[B]dx + \overline{S}A\int_{L}[B]^{T}[B]dx, \tag{10}$$

where A and L are the cross-sectional area and the length of the wire, F is the deformation gradient at the known configuration, and H is the multiplicative factor. H is the function of stress, temperature, and strain. The shorthand notation of an over-bar is used to represent the value of the variable at a known point, $\overline{x}$. By relating Equation (10) to the general truss element stiffness relation, the Young's modulus of a SMA wire can be inferred as:

$$E_{SMA} = H\overline{D}F\overline{F} + \overline{S} \tag{11}$$

SMA materials are assumed to be isotropic here and the hosting composites are assumed to be transversely isotropic. To capture the effective (or averaged) stiffness of a SMA/composite element, the new approach of a representative volume element (RVE) is adopted in this study. Figure 1 shows the RVE and its idealization procedure similar to one used in [12]. The RVE is divided into two separate cases. The constitutive equation of the case A can be described as:

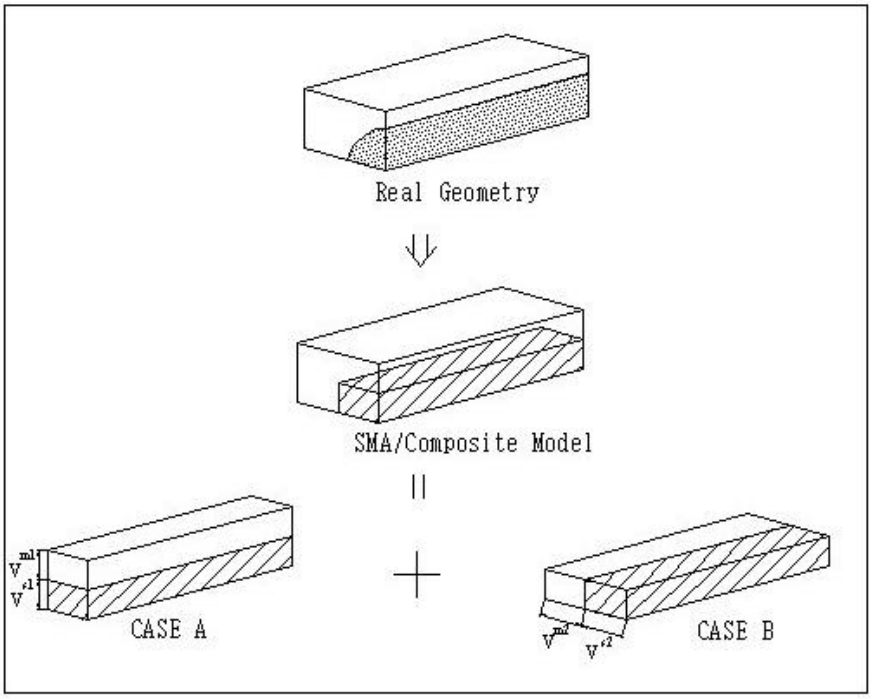

Figure 1. SMA/composite RVE model ($n^{s1,2}$ and $n^{m1,2}$ represent volume fractions.)

$$\begin{Bmatrix} s_x^{[1]} \\ s_y^{[1]} \\ s_z^{[1]} \\ t_{yz}^{[1]} \\ t_{xz}^{[1]} \\ t_{xy}^{[1]} \end{Bmatrix} = \begin{bmatrix} Q_{11}^{[1]} & Q_{12}^{[1]} & Q_{13}^{[1]} & 0 & 0 & 0 \\ Q_{12}^{[1]} & Q_{22}^{[1]} & Q_{23}^{[1]} & 0 & 0 & 0 \\ Q_{13}^{[1]} & Q_{23}^{[1]} & Q_{23}^{[1]} & 0 & 0 & 0 \\ 0 & 0 & 0 & Q_{44}^{[1]} & 0 & 0 \\ 0 & 0 & 0 & 0 & Q_{55}^{[1]} & 0 \\ 0 & 0 & 0 & 0 & 0 & Q_{55}^{[1]} \end{bmatrix} \begin{Bmatrix} e_x^{[1]} \\ e_y^{[1]} \\ e_z^{[1]} \\ g_{yz}^{[1]} \\ g_{xz}^{[1]} \\ g_{xy}^{[1]} \end{Bmatrix} \tag{12}$$

The relations of the case B can be expressed in a similar fashion to Equation (12). Then, the averaged relations combining both cases can be derived for SMA/composite materials as:

$$\begin{Bmatrix} \overline{s_x} \\ \overline{s_y} \\ \overline{s_z} \\ \overline{t_{yz}} \\ \overline{t_{xz}} \\ \overline{t_{xy}} \end{Bmatrix} = \begin{bmatrix} K_{11} & K_{12} & K_{13} & 0 & 0 & 0 \\ K_{12} & K_{22} & K_{23} & 0 & 0 & 0 \\ K_{13} & K_{23} & K_{33} & 0 & 0 & 0 \\ 0 & 0 & 0 & K_{44} & 0 & 0 \\ 0 & 0 & 0 & 0 & K_{55} & 0 \\ 0 & 0 & 0 & 0 & 0 & K_{55} \end{bmatrix} \begin{Bmatrix} \overline{e_x} \\ \overline{e_y} \\ \overline{e_z} \\ \overline{g_{yz}} \\ \overline{g_{xz}} \\ \overline{g_{xy}} \end{Bmatrix} \tag{13}$$

where K_{ij} and $Q_{ij}^{[1]}$ are the equivalent stiffnesses of a SMA/composite element. The details about stiffnesses are described in the appendix.

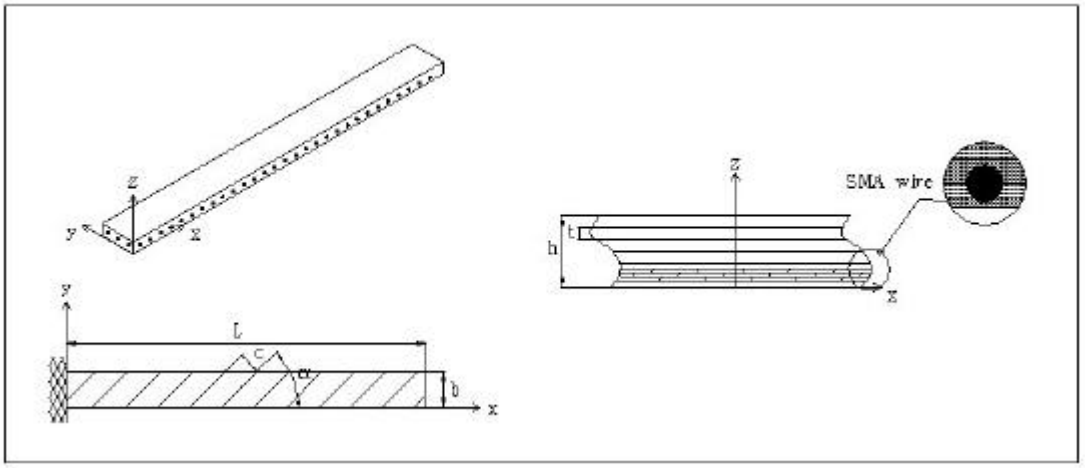

Figure 2. Schematic of a SMA/composite beam

APPLICATIONS

Numerical simulations were carried out for the shape control samples of cantilevered beams made of SMA/graphite/epoxy composites. The feature of the beam is shown in Figure 2. The mechanical properties of AS4/3501-6 and SMA wire are listed in Tables 1 and 2, respectively. Beam geometries are shown in Table 3. Due to geometric symmetry, the half was modeled with 1320 brick elements. SMA wires were embedded with four different angles a (0°, 15°, 30°, 45°) at z = 0.125 mm (i.e., between the 1st and 2nd plies from the bottom). The interval of SMA wires (c = 5 mm) was kept uniform. In all cases, initial conditions of SMA wires are e_0 = 0.0469 and T_0 = 20°C.

To validate the model, the numerical predictions of the current model were compared to Sun *et al*'s numerical results under the same conditions used in ref. [13]. The beam geometries were 50mm×5mm×500mm and seven SMA wires were embedded in hosting material (E = 30000MPa) 1.25 mm below the neutral surface. The two results are in good agreement as shown in Figure 3.

Figures 4 and 5 show the bending and axial deformations of the beam depending on electric resistive heating for the SMA wire angle, α = 0° and three layup sequences. The largest deflections (0.75 mm) were observed in this SMA angle of all cases investigated. The kinks at 40°C in the graphs are due to the transformation from martensite to austenite phases.

Figures 6-8 show the bending and twisting of the beam depending on electric resistive heating for the SMA wire angle, α = 15° and three layup sequences. Slightly different negative twists were induced depending on the layup sequences. One point of interest is that the side deflections are larger than vertical ones that are almost uniform regardless of the layup sequences.

Figures 9-11 show the bending and twisting of the beam depending on electric resistive heating for the SMA wire angle, α = 30° and three layup sequences. Similar deformation trends to α = 15° are noticed, however, larger side deflections took place. Figures 12-14 show the bending and twisting of the beam depending on electric resistant heats for the SMA wire angle, α = 45°. Interestingly enough, the reversed side deformations opposite to others are

observed. Judicious choice. These results show that the behavior of SMA/graphite/epoxy composite beam may be controlled by judicious choices of control temperatures, SMA angles, and elastic tailoring.

CONCLUSIONS

The 3-D finite element model of a SMA/graphite/epoxy beam was developed using a fully coupled constitutive model of composites and was validated by comparing with other analytical results. A new approach of capturing effective stiffnesses of SMA/composites elements was also introduced in this paper. Numerical analyses of the SMA/graphite/epoxy beam were carried out and the results indicate that the shape of SMA/graphite/epoxy composite beam may be controlled by judicious choices of resistive heating temperatures, SMA angles, and elastic tailoring. The maximum vertical deflection of 0.75 mm was induced when the SMA wires aligned along the beam length were activated. It is inferred from the numerical results that the deformations can be possibly large enough for changing the beam shape, depending on the beam geometries and the angles and locations of SMA wires. Deformations can be also easily reversed along with specially tailored layup angles.

ACKNOWLEGEDMENTS

This work was supported by Korean Research Foundation Grant (KRF-2000-003-E00026) to Cheol Kim.

REFERENCES

1. Noor, A. K., Venneri, S. L., Paul, D. B. and Hopkins, M. A., "Structures Technology for Future Aerospace Systems," *Computers and Structures*, 2000, Vol. 74, pp.507-519.
2. Tanaka, K., "A Thermomechanical Sketch of Shape Memory Effect: One Dimensional Tensile Behavior," *Res. Mechanica*, 1986, Vol. 18, pp. 251-263.
3. Liang, C. and Rogers, C. A., "One-dimensional Thermomechanical Constitutive Relations for Shape Memory Materials," *J. Intell. Mater. Syst. Struct.*, 1990, Vol. 1, pp. 207-234.
4. Brinson, L. C., "One-Dimensional Constitutive Behavior of Shape Memory Alloys: Thermomechanical Derivation with Non-Constant Material Functions and Redefined Martensite Internal Variable," *J. Intell. Mater. Syst. Struct*, 1993, Vol. 4, pp.229-242.
5. White, S. R. and Berman, J. B., "Thermomechanical Response of SMA Composite Beams with Embedded Nitinol Wires in an Epoxy Matrix," *J.of Intell.Mater.Syst.and Struct.*, 1998, Vol. 9, pp. 391-400.
6. Blonk, B. J. and Lagoudas, D. C., "Actuation of elastomeric rods with embedded two-way shape memory alloy actuators," *Smart Mater. and Struct.*, 1998, Vol. 7, pp. 771-783.
7. White, S. R. and Hebda, D. A., "Structural Behavior SMA Composite Beams," *Adaptive Material Systems*, 1995, AMD-Vol 206/MD-Vol 58, pp.111-120.
8. Epp, J. J. and Chandra, R., "Shape Memory Alloy Actuation for Active Tuning of Composite Beams," *Smart Mater. and Struct.*, 1997, Vol. 6, pp.251-264.
9. Ostachowicz, W., Krawczuk, M. and Zak, A., "Natural Frequency of Multi-Layer

Composite Plate with Embedded Shape Memory Alloy Wires," *J. of Intell. Mater. Syst. and Struct.*, 1998, Vol. 9, pp.232-237.

10. Kim, C. and White, S. R., "Thick-Walled Composite Beam Theory Including 3-D Elastic Effects and Torsional Warping," *Int. J. Solids and Struct.*, 1997, Vol. 34, pp. 4237-4259.
11. Brinson, L. C. and Lammering, R., "Finite Element Analysis of the Behavior Shape Memory Alloys and Their Applications," *Int. J. Solids and Struct.*, 1993, Vol. 3, No.23, pp. 3261-3280.
12. Bent, A. A. and Hagood, N. W., "Piezoelectric Fiber Composites with Interdigitated Electrodes," *J. of Intell. Mater. Syst. and Struct.*, 1999, Vol. 8, pp. 221-231.
13. Sun, G., Sun, S., Wu, X. and Wu, J. "A Study on thermomechanical Deformation of Elastic Beam with Embedded Shape Memory Alloy Wires," *Materials and Design*, 2000, Vol 21, pp. 525-528.

APPENDIX

The details of stiffness matrix elements in Equations (12) and (13) are:

$$Q_{11}^{[1]} = \frac{\left(Q_1^{SMA}\right)^2 - \left(Q_2^{SMA}\right)^2}{Q_1^{SMA}} v^{s1} + \frac{Q_{11}Q_{22} - Q_{12}^2}{Q_{22}} v^{m1} + \frac{Q_1^{SMA}Q_{22}}{Q_{22}v^{s1} + Q_1^{SMA}v^{m1}} \left(\frac{Q_2^{SMA}}{Q_1^{SMA}} v^{s1} + \frac{Q_{12}}{Q_{22}} v^{m1} \right)^2 \quad \text{(A1)}$$

$$Q_{22}^{[1]} = \frac{\left(Q_1^{SMA}\right)^2 - \left(Q_2^{SMA}\right)^2}{Q_1^{SMA}} v^{s1} + \frac{Q_{22}^2 - Q_{23}^2}{Q_{22}} v^{m1} + \frac{Q_1^{SMA}Q_{22}}{Q_{22}v^{s1} + Q_1^{SMA}v^{m1}} \left(\frac{Q_2^{SMA}}{Q_1^{SMA}} v^{s1} + \frac{Q_{23}}{Q_{22}} v^{m1} \right)^2 \quad \text{(A2)}$$

$$Q_{33}^{[1]} = \frac{Q_1^{SMA}Q_{22}}{Q_{22}v^{s1} + Q_1^{SMA}v^{m1}} \quad \text{(A3)}$$

$$Q_{44}^{[1]} = Q_3^{SMA}v^{s1} + Q_{44}v^{m1} \quad \text{(A4)}$$

$$Q_{55}^{[1]} = Q_3^{SMA}v^{s1} + Q_{55}v^{m1} \quad \text{(A5)}$$

$$Q_{12}^{[1]} = \frac{Q_1^{SMA}Q_2^{SMA} - \left(Q_2^{SMA}\right)^2}{Q_1^{SMA}} v^{s1} + \frac{Q_{12}Q_{22} - Q_{12}Q_{23}}{Q_{22}} v^{m1} + \frac{\left(Q_{22}Q_2^{SMA}v^{s1} + Q_1^{SMA}Q_{12}v^{m1}\right)\left(Q_{22}Q_2^{SMA}v^{s1} + Q_1^{SMA}Q_{23}v^{m1}\right)}{Q_1^{SMA}Q_{22}^2v^{s1} + \left(Q_1^{SMA}\right)^2 Q_{22}v^{m1}}$$

(A6)

$$Q_{13}^{[1]} = \frac{Q_{22}Q_2^{SMA}v^{s1} + Q_{12}Q_1^{SMA}v^{m1}}{Q_{22}v^{s1} + Q_1^{SMA}v^{m1}} \quad \text{(A7)}$$

$$Q_{23}^{[1]} = \frac{Q_2^{SMA}Q_{22}v^{s1} + Q_1^{SMA}Q_{23}v^{m1}}{Q_{22}v^{s1} + Q_1^{SMA}v^{m1}} \quad \text{(A8)}$$

$$K_{11} = \frac{Q_{11}^{[1]}Q_{22}^{[1]} - \left(Q_{12}^{[1]}\right)^2}{Q_{22}^{[1]}} v^{s2} + \frac{Q_{11}Q_{22} - Q_{12}^2}{Q_{22}} v^{m2} + \frac{Q_{22}^{[1]}Q_{22}}{Q_{22}v^{s2} + Q_{22}^{[1]}v^{m2}} \left(\frac{Q_{23}^{[1]}}{Q_{22}^{[1]}} v^{s2} + \frac{Q_{12}}{Q_{22}} v^{m2} \right)^2 \quad \text{(B1)}$$

$$K_{22}=\frac{\left(Q_{22}^{[1]}\right)^2-\left(Q_{23}^{[1]}\right)^2}{Q_{22}^{[1]}}v^{s2}+\frac{Q_{22}^2-Q_{23}^2}{Q_{22}}v^{m2}+\frac{Q_{22}^{[1]}Q_{22}}{Q_{22}v^{s2}+Q_{22}^{[1]}v^{m2}}\left(\frac{Q_{23}^{[1]}}{Q_{22}^{[1]}}v^{s2}+\frac{Q_{23}}{Q_{22}}v^{m2}\right)^2 \quad \text{(B2)}$$

$$K_{33}=\frac{Q_{22}^{[1]}Q_{22}}{Q_{22}v^{s2}+Q_{22}^{[1]}v^{m2}} \quad \text{(B3)}$$

$$K_{44}=v^{s2}Q_3^{SMA}+v^{m2}Q_{44} \quad \text{(B4)}$$

$$K_{55}=v^{s2}Q_3^{SMA}+v^{m2}Q_{55} \quad \text{(B5)}$$

$$K_{12}=\frac{Q_{12}^{[1]}Q_{22}^{[1]}-Q_{12}^{[1]}Q_{23}^{[1]}}{Q_{22}^{[1]}}v^{s2}+\frac{Q_{12}Q_{22}-Q_{12}Q_{23}}{Q_{22}}v^{m2}+\frac{\left(Q_{22}Q_{23}^{[1]}v^{s2}+Q_{22}^{[1]}Q_{12}v^{m2}\right)\left(Q_{22}Q_{23}^{[1]}v^{s2}+Q_{23}Q_{22}^{[1]}v^{m2}\right)}{Q_{22}^2Q_{22}^{[1]}v^{s2}+\left(Q_{22}^{[1]}\right)^2Q_{22}v^{m2}} \quad \text{(B6)}$$

$$K_{13}=\frac{Q_{22}Q_{23}^{[1]}v^{s2}+Q_{22}^{[1]}Q_{12}v^{m2}}{Q_{22}v^{s2}+Q_{22}^{[1]}v^{m2}} \quad \text{(B7)}$$

$$K_{23}=\frac{Q_{22}Q_{23}^{[1]}v^{s2}+Q_{22}^{[1]}Q_{23}v^{m2}}{Q_{22}v^{s2}+Q_{22}^{[1]}v^{m2}} \quad \text{(B8)}$$

where Q_{ij} and Q_{ij}^{SMA} denote the stiffness components of matrix and SMA, respectively.

Table 1. Material properties for SMA

Moduli	Temperature	Transformation Constant	Strain
$D_a=67\times10^3\,MPa$	$M_f=9°C$	$C_M=8MPa°C^{-1}$	$e_L=0.067$
$D_M=26.3\times10^3\,MPa$	$M_s=18.4°C$	$C_A=13.8MPa°C^{-1}$	$e_0=0.0469$
$\Theta=0.55\times10^3\,MPa°C$	$A_s=34.5°C$	$s_s^{cr}=100MPa$	
$n=0.33$	$A_f=49°C$	$s_f^{cr}=170MPa$	

Table 2. Mechanical properties of AS4/3501-6

$E_{11}=141.96GPa$	$E_{22}=E_{33}=9.76GPa$
$G_{12}=G_{13}=6.0GPa$	$G_{23}=4.83GPa$
$n_{12}=n_{13}=0.24$	$n_{23}=0.5$

Table 3. Beam dimensions (mm)

Length (L)	300
Width (b)	30
Radius of a SMA wire	0.1
Thickness (h)	0.75

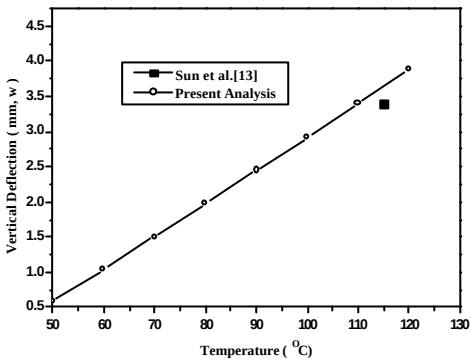

Figure 3. Vertical deflections with temperatures for a validation study.

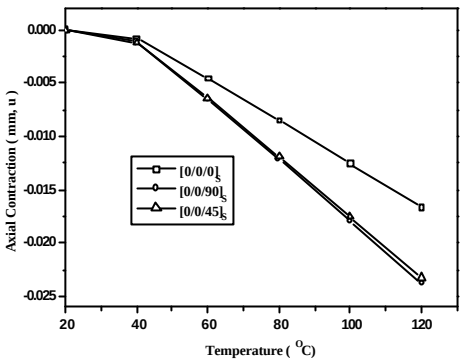

Figure 4. Axial contractions of a beam tip with controlling temperatures (α = 0°)

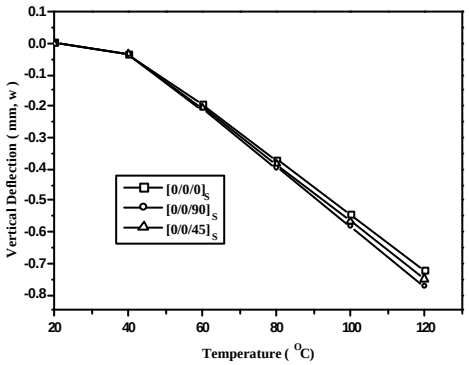

Figure 5. Deflections of a beam tip with controlling temperatures (α = 0°)

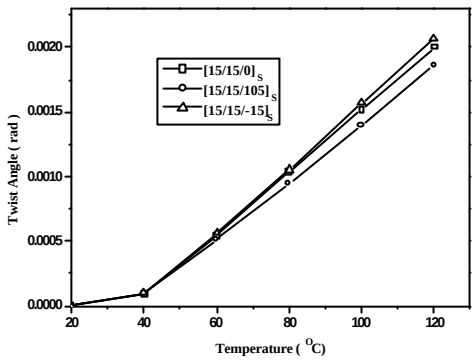

Figure 6. Twist angles with controlling temperatures (α = 15°)

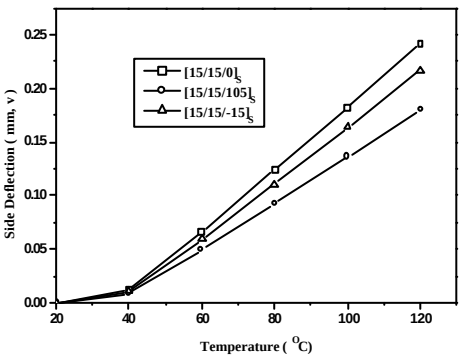

Figure 7. Side deflections of a beam tip with controlling temperatures (α = 15°)

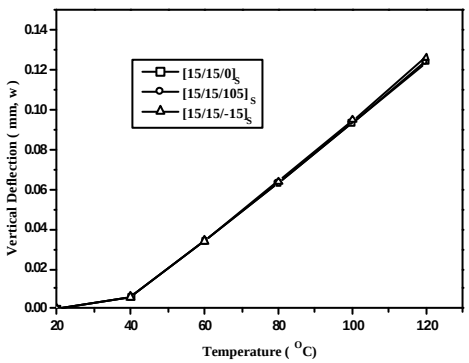

Figure 8. Vertical deflections of a beam tip with controlling temperatures (α = 15°)

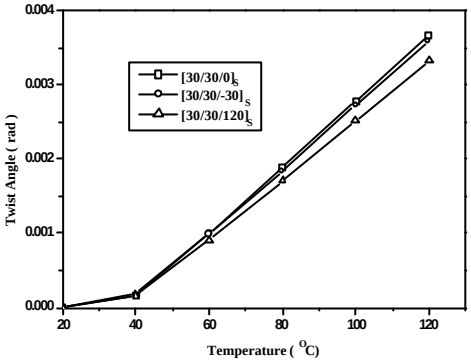

Figure 9. Twist angles with controlling temperatures (α = 30°)

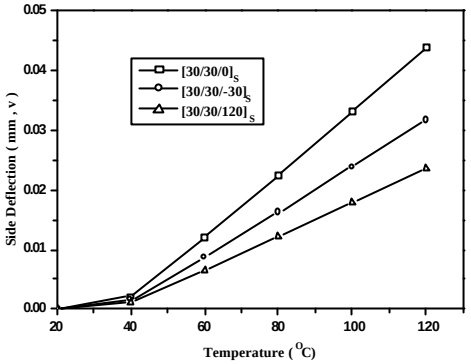

Figure 10. Side deflections of a beam tip with controlling temperatures (α = 30°)

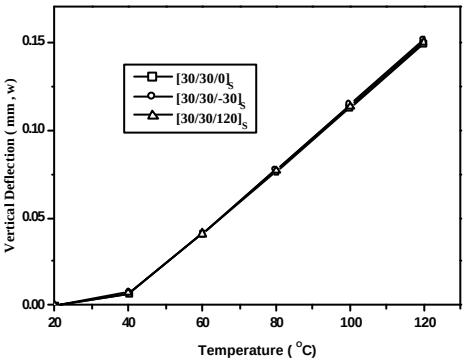

Figure 11. Vertical deflections of a beam tip with controlling temperatures (α = 30°)

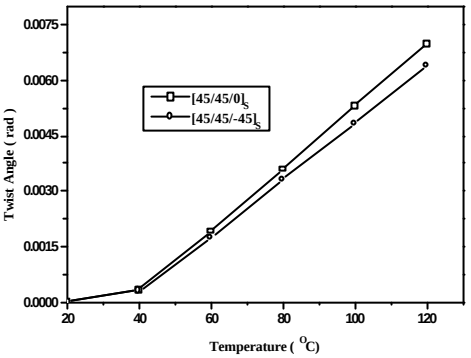

Figure 12. Twist angles with controlling temperatures (α = 45°)

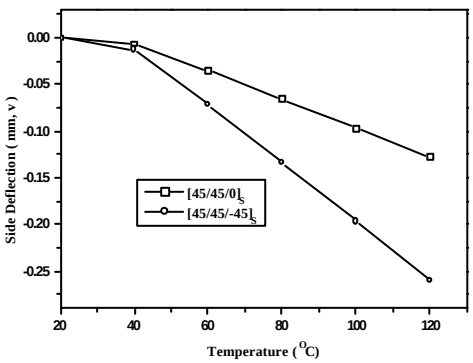

Figure 13. Side deflections of a beam tip with controlling temperatures (α = 45°)

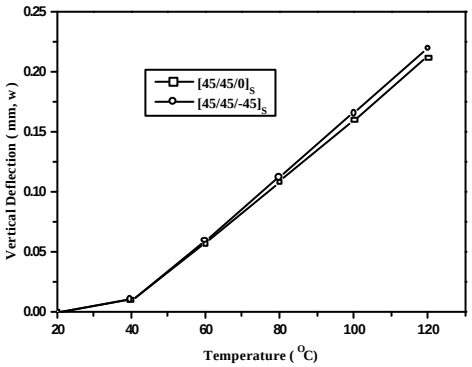

Figure 14. Vertical deflections of a beam tip with controlling temperatures (α = 45°)